Automated Quantification of the Relation between Resistor-capacitor Subcircuits from an Impedance Spectrum

Thomas Schmid[1], Dorothee Günzel[2] and Martin Bogdan[1]
[1]*Department of Computer Engineering, Universität Leipzig, Augustusplatz 10, D-04109 Leipzig, Germany*
[2]*Institute of Clinical Physiology, Campus Benjamin Franklin, Charité, D-12220 Berlin, Germany*

Keywords: Impedance Spectroscopy, Epithelia, HT-29/B6, IPEC-J2, Machine Learning, Feature Selection, Decision Trees, Artificial Neural Networks, Random Forests.

Abstract: In epithelial physiology, it is common to use an equivalent electric circuit with two resistor-capacitor (RC) subcircuits in series as a model for the electrical behavior of body cells. The relation between these two subcircuits can be quantified by a quotient of their time constants τ. While this quotient is a direct indicator of the shape of impedance spectra, its value cannot be determined directly. Here, we suggest a machine learning-based approach to predict the τ quotient from impedance spectra. We perform systematic extraction of statistical features, algorithmic feature ranking and dimension reduction on model impedance spectra derived from tissue-equivalent electric circuits. Our results demonstrate that this quotient can be predicted reliably enough from implicit features to discriminate semicircular against non-semicircular impedance spectra.

1 INTRODUCTION

Characterization of current through a given sample is of interest not only in electric engineering, but also in many biomedical applications. Often, like in physiological analyses of epithelial cells, this is achieved by applying alternating current (AC) and measuring the opposition to this current, called impedance. As the applied frequencies are varied across a given spectrum, this concept is commonly refered to as impedance spectroscopy.

When applied to epithelial cell layers, this allows to discriminate alternative current pathways (Krug et al., 2009). While these layers form barriers between compartments of an organism, they also regulate exchange of ions, water and nutrients. At their apical side, epithelia are joined by the tight junction (TJ), which regulates ion transport between neighbouring cells (paracellularly). Alternatively, ions may be transported through the cells (transcellularly), i.e. across the apical and basolateral cell membrane. Both pathways may be altered under physiological and pathophysiological conditions.

For simple epithelia that consist of a single layer of cells, electrical properties can be described by an equivalent electric circuit as depicted in Figure 1a (Günzel et al., 2012). Within this 5-parameter circuit, the TJ is represented by a resistor R_p, whereas each side of the epithelium is characterized by an RC subcircuit, a or b, respectively. Each subcircuit is readily described by its time constant $\tau_a = R_a \cdot C_a$ and $\tau_b = R_b \cdot C_b$ respectively. The ratio between the numerically larger time constant and the numerically smaller time constant establishes a good quantification of differing electrical properties of the apical and basolateral membrane, as e.g. caused by the activation of ion channels. With known resistor and capacitor values, this relation is given by the quotient $q = \frac{\tau_1}{\tau_2}$ where $\tau_1, \tau_2 \in \{\tau_a, \tau_b\}$ and $\tau_1 > \tau_2$.

For measured impedance spectra, however, neither the time constants nor q are known. Due to the symmetric organization of the subcircuits and the ambivalence of the resulting spectra, values of the underlying resistors and capacitors cannot be determined reliably from a single spectrum. And while q serves as a direct indicator whether the spectrum is of semicircular or non-semicircular shape, this exact relation has not been understood so far.

In previous work, we have modeled realistic impedance spectra for two distinct epithelial cell lines (Schmid et al., 2013a). Thereby, relevant electrical properties were determined by predicting x-axis intercepts from explicitly measured data. In a next step, we extracted implicit statistical features of ideal spectra, applied algorithmic feature selection and evaluated feature subsets with artificial neural networks

Schmid T., Günzel D. and Bogdan M..
Automated Quantification of the Relation between Resistor-capacitor Subcircuits from an Impedance Spectrum.
DOI: 10.5220/0004746501410148
In *Proceedings of the International Conference on Bio-inspired Systems and Signal Processing* (BIOSIGNALS-2014), pages 141-148
ISBN: 978-989-758-011-6

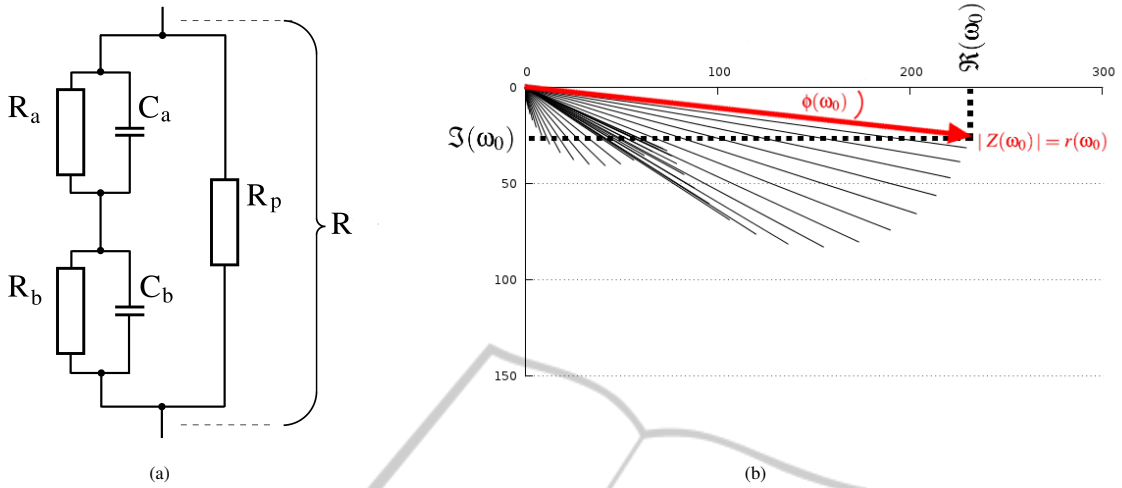

(a) (b)

Figure 1: (a) Equivalent electric circuit discriminating between apical ($\tau_a = R_aC_a$) and basolateral ($\tau_b = R_bC_b$) properties of an epithelial cell layer. (b) An impedance spectrum reflecting AC application at 42 frequencies between 1.3 and 16,000 Hz on an epithelial cell layer with low resistance $R = R_p(R_a+R_b)/(R_p+R_a+R_b)$. In contrast to physiological conditions (where $\tau_a \approx \tau_b$), here R_a is decreased considerably by drug application. Thus, τ_a decreases and a non-semicircular shape is obtained. Impedances Z can be displayed as complex numbers $(\Re, \Im)$ or in polar coordinates (magnitude r, phase ϕ).

(ANNs) (Schmid et al., 2013b). Here, we continue to further systemize this approach. For the more complex task of predicting q, we extract more implicit features, perform dimension reduction and task differentiation, and compare concurring machine learning techniques. As no conventional way to estimate q exists, we use decision trees as baseline method.

2 METHODS

2.1 Modeling Impedance Spectra and Extracting Statistical Features

The complex impedance Z of the tissue-equivalent electric circuit (Figure 1a) at an angular frequency ω can be derived by Kirchhoff's laws from the impedances of its components R_a, C_a, R_b, C_b and R_p:

$$Z(\omega) = \frac{R_p(R_a+R_b)+i\omega[R_p(R_a\tau_b+R_b\tau_a)]}{R_a+R_b+R_p(1-\omega^2\tau_a\tau_b)+i\omega[R_p(\tau_a+\tau_b)+R_a\tau_b+R_b\tau_a]} \quad (1)$$

where $i = \sqrt{-1}$, and $\tau_a = R_aC_a$ and $\tau_b = R_bC_b$.

In measurements, a spectrum of n impedances $Z(\omega_0),\ldots,Z(\omega_{n-1})$, i.e. n tupels of real and imaginary parts $((\Re(\omega_0),\Im(\omega_0)),\ldots,(\Re(\omega_{n-1}),\ \Im(\omega_{n-1})))$, is obtained by applying AC at n frequencies. Alternatively, the complex impedances can be transformed into polar coordinates, i.e. into phase ϕ and magnitude r $(((\phi(\omega_0),r(\omega_0)),\ldots,(\phi(\omega_{n-1}),r(\omega_{n-1}))))$.

In the following, phases and magnitudes of a spectrum are handled as separate feature sets S_ϕ and S_r:

$$S_\phi = \{\phi(\omega_0),\ldots,\phi(\omega_{n-1})\} \quad (2)$$

$$S_r = \{r(\omega_0),\ldots,r(\omega_{n-1})\} \quad (3)$$

Analogously for real and imaginary parts:

$$S_\Re = \{\Re(\omega_0),\ldots,\Re(\omega_{n-1})\} \quad (4)$$

$$S_\Im = \{\Im(\omega_0),\ldots,\Im(\omega_{n-1})\} \quad (5)$$

From these four feature sets, new sets of inherent features are created that represent the $n-1$ distances between two consecutive features of the original sets:

$$S_{\Delta\phi} = \{\Delta\phi|\Delta\phi_i = \phi(\omega_{i+1})-\phi(\omega_i), 0 \le i < n-1\} \quad (6)$$

$$S_{\Delta r} = \{\Delta r|\Delta r_i = r(\omega_{i+1})-r(\omega_i), 0 \le i < n-1\} \quad (7)$$

$$S_{\Delta\Re} = \{\Delta\Re|\Delta\Re_i = \Re(\omega_{i+1})-\Re(\omega_i), 0 \le i < n-1\} \quad (8)$$

$$S_{\Delta\Im} = \{\Delta\Im|\Delta\Im_i = \Im(\omega_{i+1})-\Im(\omega_i), 0 \le i < n-1\} \quad (9)$$

Additionally, forward ($\overrightarrow{\delta}$) and backward ($\overleftarrow{\delta}$) differential quotients were calculated from real and imaginary parts of neighbouring impedances:

$$S_{\overrightarrow{\delta}} = \left\{\overrightarrow{\delta}\,|\,\overrightarrow{\delta}_i = \frac{\Im(\omega_{i+1})-\Im(\omega_i)}{\Re(\omega_{i+1})-\Re(\omega_i)}, 0 \le i < n-1, \omega_i < \omega_{i+1}\right\} \quad (10)$$

$$S_{\overleftarrow{\delta}} = \left\{\overleftarrow{\delta}\,|\,\overleftarrow{\delta}_i = \frac{\Im(\omega_{i+1})-\Im(\omega_i)}{\Re(\omega_{i+1})-\Re(\omega_i)}, 0 \le i < n-1, \omega_i > \omega_{i+1}\right\} \quad (11)$$

For each of these sets of explicit spectrum features, a total of 16 univariate statistical parameters were calculated (see Appendix A for details). While the explicit features were discarded at this point, the extracted sets of implicit features were used in three variants: in absolute values, normalized to the respective mean, and normalized to the respective median; due to the fact that differential quotients are already

Table 1: Characteristics of the modeled datasets.

Dataset		Cases	Target q					
			Minimum	1st Quantile	Median	Mean	3rd Quantile	Maximum
HT-29/B6	unaltered	299,112	2.02	15.64	33.00	2983.09	109.19	89310.1
	drugged	151,043	1.55	15.17	31.88	1988.03	101.85	88425.9
IPEC J2	unaltered	458,326	1.00	2.18	3.32	4.38	5.35	31.74
	drugged	279,268	1.01	2.18	3.31	4.38	5.34	31.39
Combined		1,187,750	1.00	2.79	5.60	1006.77	20.68	89310.1
	Training	791,834	1.00	2.79	5.61	1005.00	20.78	89310.0
	Test	395,916	1.01	2.79	5.58	1011.00	20.50	86220.0

relative parameters by nature, datasets $S_{\overrightarrow{\delta}}$ and $S_{\overleftarrow{\delta}}$ were only used in absolute values. This yielded a total of 26 extracted feature sets, consisting of a total of 416 implicit spectrum features.

By varying the underlying five circuit parameters, measurements on distinct epithelial cell lines under a variety of experiment conditions can be mimicked (Schmid et al., 2013b; Schmid et al., 2013a). Here, we imitated the epithelial cell lines HT-29/B6 and IPEC-J2, for which we have described electrical properties before and after application of parameter-altering drugs previously (Schmid et al., 2013a). These distinct data sets from each cell line under each condition were combined before the following analyses in order to gain cell line-independet results (Table 1). Note that for simplicity, the scatter resulting from real-world measurements is not modeled here.

2.2 Assessing the Complexity of the Regression Task

As baseline method for predicting q and to obtain a first glance at the complexity of regression task, we applied decision trees[1]. The combined data was split into a training dataset (66 percent) and a test dataset (33 percent), where both datasets showed comparable statistical characteristics (Table 1). For complexity analysis, the number of cases from the training dataset used for building the tree was increased stepwise (starting at 1 percent of the training dataset) while the test dataset was left unaltered.

Further, we investigated whether complexity of the regression task can be reduced by splitting it into intuitive subtasks. Based on the target domain, two splittings were tested. In the one variant, we discriminated between semicircular ($q < 5$) and non-semicircular ($q > 5$) spectra (Schmid et al., 2013b). In the other variant, we divided the target domain into five distinct logarithmic target domains.

[1]All decision tree tasks were performed with *R* and the standard package *tree* by B. Ripley.

2.3 Searching for Predictive Feature Subsets

As no ideal feature selection approach is known for this specific task, three alternatives were tested:

- Variables used by decision trees were taken as feature subsets. For a tree built without splitting, this implied a set of 5 features (termed subset A). For trees built for the two-fold splitting, both feature subsets were merged, yielding a set of 13 unique features (subset B). For trees built for the five-fold splitting, merging all feature subsets yielded a set of 23 unique features (subset C).
- All 416 features were ranked by a nearest neighbor-based algorithm. In contrast to filter methods, which rank features individually, the here used "regression gradient feature selection"[2] evaluated the performance of a feature within a feature subset (Navot et al., 2005). In order to determine an optimal subset size, subsets of the 5, 10, 15, 20 and 25 top-ranked features were evaluated. These features are referred to as subset D.
- Random forests were used to determine importance of all 416 variables[3]. Aggregating output of a large number of decision trees, Random Forests provide relatively unbiased predictions (Breiman, 2001). Again, subsets of the 5, 10, 15, 20 and 25 top-ranked features were evaluated (subset E).

For all candidate feature subsets (A, B, C, D, E), the combined dataset (Table 1) was reduced to the respective features, split into logarithmic target subdomains and assessed by decision trees, multi-layer perceptrons (MLPs)[4], and random forests.

[2]All RGS rankings were performed with MATLAB and MATLAB code provided by the algorithm authors online at www.cs.huji.ac.il/labs/learning/code/fsr/

[3]All random forest tasks were performed with *R* and the package *randomForest* (Liaw and Wiener, 2002).

[4]For all MLPs, we use a n-2-1 architecture with one hidden layer consisting of two hidden units. Training was performed by backpropagation and using the FORWISS Artificial Neural Network Toolbox (Arras and Mohraz, 1996).

2.4 Searching for Subtasks by Feature Subset-Specific Clustering

As an alternative to relying on q for task differentiation (Section 2.2), we also tested splitting the regression task into subtasks solely with respect to individual feature subsets. Due to the multi-dimensionality of the feature domains, however, such splittings cannot be defined intuitively or by domain knowledge. Therefore, for each feature subset, we performed k-means clustering based on the respective features[5]. In all clusterings, the within groups sum of squares was determined for $n = \{2, ..., 15\}$ clusters.

In parallel, such analyses were also performed for those initial feature sets $S \in \{S_\phi, S_r, S_\Re, S_\Im, ...\}$ that could be considered relevant based on the previous feature selection and ranking. Feature sets were assumed to be relevant for predicting q if two or more of its features did appear in any of the previously identified feature subsets (Section 2.3).

For the feature subset and feature set that showed the lowest group sums of squares, clusterings were assessed in more detail. Analogously to previous evaluations, spectra of each cluster were separated into training (66 percent) and test (33 percent) data and evaluated by Random Forests. By this, mean test errors of the various clusterings could be compared.

3 RESULTS

3.1 Complexity Analysis

With increasing number of training cases, no considerable improvement of the test error was observed. In particular, even the mean absolute derivation from the target q, was measured throughout to be considerably larger than a hundred percent of the target (Figure 2). Complexity is here measured as number of variables used by the respective decision tree. While no decrease of the complexity was observed relative to using five percent of the training datasets, the actually used variables changed with increasing percentage.

When discriminating between semicircular and non-semicircular spectra, a much lower mean absolute derivation from the target was observed for semicircular spectra (Table 2); the same holds true for the maximum derivation. Logarithmically splitting the target domain yielded mean absolute derivations between 18 and 49 percent (Table 3); maxium derivations, however, lay between 215 and 420 percent.

[5]All k-means clusterings were performed with *R* and its built-in function *kmeans*.

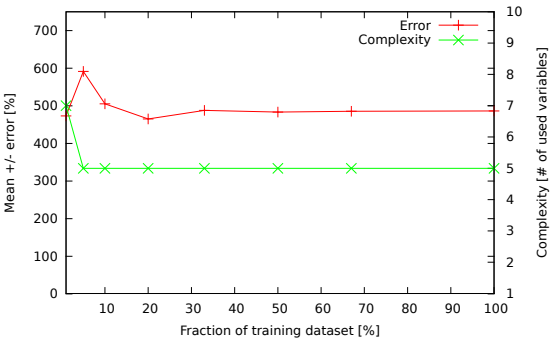

Figure 2: Development of mean error [±%] and complexity (number of used variables) by size of training data.

Table 2: Error for shape-based splitting (target domain).

Target q	**Test Error** [+/- %]		
Range	Minimum	Mean	Maximum
1.0 - 5.0	0.0	16.3	164.9
5.0 - 89,310	0.0	531.0	333,400.0

Table 3: Error for logarithmic splitting (target domain).

Target q	**Test Error** [+/- %]		
Range	Minimum	Mean	Maximum
1 - 10	0.0	23.2	238.1
10 - 100	0.0	26.7	419.5
100 - 1,000	0.0	19.0	272.7
1,000 - 10,000	0.0	48.7	410.3
10,000 - 89,310	0.0	37.9	216.5

Note that splitting was applied to the combined data (Table 1); the results were, again, divided into training (66 percent) and test (33 percent) data.

3.2 Predictiveness of Feature Subsets

As described, a total of 13 differing potential predictors were tested with decision trees, ANNs and random forests. Tests were performed separately for each of the five logarithmic ranges of the target q (cf. Table 3). As decisions trees, however, did in all applications not perform notably better than previously with all 416 features (cf. Table 3), we only show ANN and random forest results for feature subsets A, B, C and the best D and best E subset (Tables 4-8). Error of the predictions is given as the absolute derivation from the target relative to the respective target.

Neither MLPs nor random forests reached test error of less than ten percent for the full target range, i.e. not under all five conditions tested. Using MLPs, a mean error of less than ten percent could not be achieved with any of the feature subsets; best mean errors were observed for feature subset B in the target range $100 < q < 1000$ (16.4 percent) and for feature subset C in the target range $100 < q < 1000$ (14.6 percent).

Table 4: Absolute deviation (+/-) from the target q for feature subset A [%].

Target	**ANN**						**Random Forest**					
Range	Min.	1.Qrt.	Med.	Avg.	3.Qrt.	Max.	Min.	1.Qrt.	Med.	Avg.	3.Qrt.	Max.
1-10	0.0	18.2	37.2	55.1	74.2	420.7	0.0	4.1	8.8	12.4	15.7	209.7
10-100	0.0	15.1	32.4	40.9	56.6	353.7	0.0	6.9	15.8	20.4	29.0	170.7
100-1000	0.0	8.0	18.0	30.5	32.5	477.4	0.0	3.1	6.7	9.3	12.1	261.9
1000-10000	0.0	15.4	33.5	59.7	72.7	511.5	0.0	12.8	30.8	44.9	55.0	459.7
>10000	0.0	15.5	31.8	41.5	56.9	188.4	0.0	14.3	29.0	36.1	46.0	337.8

Table 5: Absolute deviation (+/-) from the target q for feature subset B [%].

Target	**ANN**						**Random Forest**					
Range	Min.	1.Qrt.	Med.	Avg.	3.Qrt.	Max.	Min.	1.Qrt.	Med.	Avg.	3.Qrt.	Max.
1-10	0.0	7.7	17.9	29.6	37.9	435.2	0.0	1.5	3.4	5.1	6.7	181.5
10-100	0.0	12.6	26.5	39.8	49.2	558.7	0.0	4.3	10.0	14.1	19.7	156.4
100-1000	0.0	6.3	13.0	16.4	21.5	140.4	0.0	0.4	1.0	3.9	2.6	212.9
1000-10000	0.0	14.7	34.1	59.3	70.8	428.6	0.0	12.2	29.7	44.7	55.3	575.6
>10000	0.0	14.9	28.4	37.2	45.5	361.4	0.0	14.2	28.8	36.6	46.2	339.0

Table 6: Absolute deviation (+/-) from the target q for feature subset C [%].

Target	**ANN**						**Random Forest**					
Range	Min.	1.Qrt.	Med.	Avg.	3.Qrt.	Max.	Min.	1.Qrt.	Med.	Avg.	3.Qrt.	Max.
1-10	0.0	8.2	18.7	30.5	38.1	525.3	0.0	1.5	3.3	4.9	6.4	93.4
10-100	0.0	9.7	21.5	29.0	38.1	878.8	0.00	3.9	9.2	13.5	18.9	127.0
100-1000	0.0	5.5	11.3	14.6	19.0	163.8	0.0	0.6	1.4	4.1	3.3	178.1
1000-10000	0.0	13.7	32.9	56.4	63.8	399.6	0.0	11.9	28.6	43.5	52.9	569.6
>10000	0.0	14.6	28.9	37.1	44.9	413.6	0.0	13.2	27.1	34.0	43.3	365.6

Table 7: Absolute deviation (+/-) from the target q for the top 15 features of subset D (D.15) [%].

Target	**ANN**						**Random Forest**					
Range	Min.	1.Qrt.	Med.	Avg.	3.Qrt.	Max.	Min.	1.Qrt.	Med.	Avg.	3.Qrt.	Max.
1-10	0.0	9.1	19.6	32.3	36.1	507.6	0.0	2.4	5.1	6.6	9.1	230.4
10-100	0.0	10.0	22.5	32.0	41.5	383.6	0.0	4.6	10.3	14.6	20.1	155.6
100-1000	0.0	5.2	10.6	14.5	17.3	162.8	0.0	0.4	0.9	3.7	2.4	205.1
1000-10000	0.0	13.9	33.0	57.6	65.4	385.4	0.0	12.1	29.7	44.9	54.7	557.9
>10000	0.0	15.1	29.2	37.7	45.8	354.3	0.0	14.2	28.6	36.6	46.1	352.4

Table 8: Absolute deviation (+/-) from the target q for the top 20 features of subset E (E.20) [%].

Target	**ANN**						**Random Forest**					
Range	Min.	1.Qrt.	Med.	Avg.	3.Qrt.	Max.	Min.	1.Qrt.	Med.	Avg.	3.Qrt.	Max.
1-10	0.0	11.5	24.6	37.1	47.8	466.5	0.0	2.5	5.3	7.4	9.8	277.6
10-100	0.0	9.8	21.9	28.4	38.2	463.8	0.0	4.5	10.5	14.4	20.0	184.1
100-1000	0.0	6.9	14.1	17.4	21.8	222.9	0.0	1.0	2.1	4.9	4.5	167.2
1000-10000	0.0	14.0	32.9	57.7	66.3	550.3	0.0	12.3	29.0	43.7	53.2	553.2
>10000	0.0	15.0	29.1	37.6	45.9	276.1	0.0	13.6	27.2	34.1	43.2	374.5

While random forests performed comparably to MLPs in the two largest target ranges ($q > 1000$), test error was constantly lower for the remaining ranges ($q < 1000$). Except for feature subset A, mean error for these three subtasks lay constantly below 15 percent. Best overall mean errors were observed for subset C with 4.9 percent (target range $1 < q < 10$), 13.5 percent ($10 < q < 100$) and 4.1 percent ($100 < q < 1000$).

3.3 Regression Subtasks by Clustering Feature Subsets

Cluster analysis of the feature domain showed that for all feature subsets (Figure 3a) and relevant feature sets (Figure 3b) the within-group-sum-of-squares decreases rapidly (Figure 3a, 3b). Using more than ten clusters, this did not decrease notably further for any of the subsets or sets. Among subsets, the lowest within-group-sum-of-squares is observed for subset D.5, containing the 5 features top-ranked by the

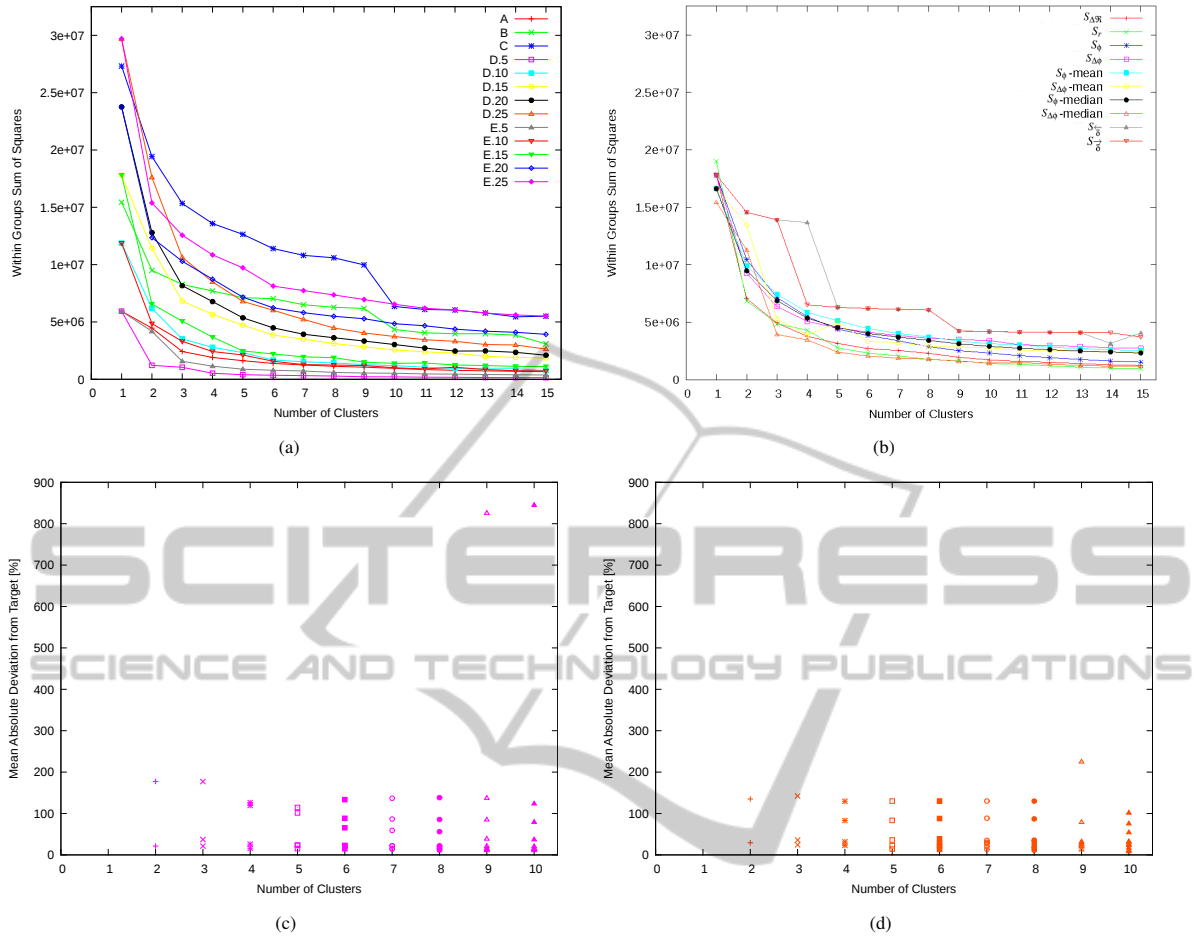

Figure 3: (a) Within group sum of squares for clusters of feature subsets A, B, C, D and E plotted against the number of clusters n. (b) Within group sum of squares for clusters of initial feature sets S where at least two features were part of the feature subsets A, B or C, or were top-ranked by RGS (subset D) or Random Forests (subset E). (c) Error of predictions when clustering training data consisting of the five top-ranked features of subset D (D.5) into n clusters. Each cluster is trained and tested individually by Random Forests. Mean deviations from target q [$\pm$%] are displayed per cluster. (d) Error of predictions when clustering training data based consisting of the median-normalized features of feature set $S_{\Delta\phi}$ into n clusters. Each cluster is trained and tested individually by Random Forests. Mean deviations from target q [$\pm$%] are displayed per cluster.

RGS algorithm. Among sets, none gained a value as low as feature subset D.5. The best-performing set was median-normalized $S_{\Delta\phi}$.

Training and predicting q based on individual clusters of feature subset D.5 (Figure 3c) or of median-normalized feature set $S_{\Delta\phi}$ (Figure 3d) respectively, showed no convergence of the test errors per clustering. In particular, for all tested clusterings at least one of the clusters exhibited a mean test error of more than hundred percent. Maximum error of an individual cluster was 845.5 percent for D.5 with $n = 10$ clusters and 225.5 percent for median-normalized feature set $S_{\Delta\phi}$ with $n = 9$ clusters.

4 DISCUSSION

4.1 Complexity of the Regression Task

Using an increasing portion of the training data to predict q with decision trees showed that even with a very large number of training vectors, q can not be predicted with satisfying precision (Figure 2). As we had to split similar regression tasks on impedance data into size-dependent (Schmid et al., 2013a) or shape-dependent (Schmid et al., 2013b) subtasks in previous work, this is not particularly surprising. For the present task, however, neither of these approaches were adequate. On the one hand, splitting according

to the spectrum size was not reasonable here, as q is a size-independent variable. Splitting the task into subtasks for semicircular ($q < 5$) and non-semicircular spectra ($q > 5$), on the other hand, was tested but did not solve the problem (cf. Table 2).

As an intuitive alternative, a logarithmic split of the target domain into subdomains of varying range was tested. This approach is based on the rationale that spectra with very large q are less frequently observed in practice as well as in the modeled datasets. Compared to initial results (Figure 2), significantly lower error rates were observed when using decision trees (Table 3) and reasonable error rates in 3 out of 5 subtasks ($q < 1000$) when using random forests (Table 5 and 6). For the lowest target range ($1 < q < 10$), random forests showed a satisfying mean error of mostly less than ten percent, when applied to subset C of even less than five percent.

4.2 Predictiveness of Feature Subsets

Evaluation of the 13 potentially predictive feature subsets identified by the three distinct approaches showed that at a number of five features (subsets A, D.5, E.5) is likely not enough for precise predictions. For ANNs as well as for Random Forests, using subsets with ten or more features showed lesser mean error (cf. Table 4-8). We take this, again, as an indicator that the given task is of complex nature.

Training Random Forests with subset C, a relatively high precision of predictions is observed for the target range $1 < q < 10$. Not only is the mean error lesser than five percent, but also is the third quantile lesser than ten percent (Table 6). Similarily to observations on other feature subsets, however, the maximum error was considerably larger than that (here: 93.4 percent). While this deviation is currently too extreme for practical applications, we are convinced that such extreme errors can be reduced in future work.

An obvious trend among all predictions was the fact that Random Forests did perform generally better than ANNs. While some improvement might be possible here with more complex ANN architectures, we take the obtained results as a trend indicating advantages in using Random Forests.

4.3 Target-specific versus Feature Subset-specific Task Differentiation

Clustering based on statistical features of impedance spectra is possible for subsets A, B, C, D, E (Figure 3a) as well as for the initial feature sets S (Figure 3b). While the variance of the within groups sum of squares is in general greater among the subsets than among the sets, even the best performing subset (top-ranked 15 features of subset D, D.15) shows a relatively large within groups sum of squares.

For subset D.15, training and testing individually for each cluster yielded considerably larger mean errors than using logarithmic subdomains of q (Figure 3c). This effect seems not to dependent on the number of clusters and was observed similarly when training individually for each cluster of the best-performing feature set (median-normalized $S_{\Delta\phi}$, Figure 3d). For the given regression task, deriving subtasks based on the target q therefore appears to be more fruitful than deriving subtasks from the feature domain. In practice, however, matching measured spectra to such subtasks would require a previous classification step.

5 CONCLUSIONS

With the present study, we aimed at understanding the nature of the relation between the τ quotient q and the shape of an impedance spectrum obtained from the given five-parameters electric circuit (Figure 1b). Based on ideally modeled spectra, we found that the task of predicting q from statistical features inherent in each spectrum is of such complex nature that is has to be further differentiated. Our results imply that deriving substasks by splitting the target domain is more effective than deriving subtasks with respect to feature subset clusters.

When dividing the target domain into logarithmic subdomains, we found that a relatively small number of statistical features is sufficient for reasonable predictions of q values $<$1000. Moreover, we could show for values $<$10 that q can be estimated with a satisfying mean error of less than five percent. As q indicates in this particular range whether the spectrum possesses a semicircular or a non-semicircular shape, this result provides a basis for an automated discrimination between these two spectrum types.

REFERENCES

Arras, M. K. and Mohraz, K. (1996). *FORWISS Artificial Neural Network Simulation Toolbox v.2.2*. Bayerisches Forschungszentrum für wissensbasierte Systeme, Erlangen, Germany.

Breiman, L. (2001). Random forests. *Machine learning*, 45(1):5–32.

Günzel, D., Zakrzewski, S. S., Schmid, T., Pangalos, M., Wiedenhoeft, J., Blasse, C., Ozboda, C., and Krug, S. M. (2012). From ter to trans-and paracellular resistance: lessons from impedance spectroscopy. *Annals*

of the New York Academy of Sciences, 1257(1):142–151.

Krug, S. M., Fromm, M., and Günzel, D. (2009). Two-path impedance spectroscopy for measuring paracellular and transcellular epithelial resistance. *Biophys J*, 97(8):2202–2211.

Liaw, A. and Wiener, M. (2002). Classification and regression by randomforest. *R news*, 2(3):18–22.

Navot, A., Shpigelman, L., Tishby, N., and Vaadia, E. (2005). Nearest neighbor based feature selection for regression and its application to neural activity. *Advances in Neural Information Processing Systems (NIPS)*, 19.

Schmid, T., Bogdan, M., and Günzel, D. (2013a). Discerning apical and basolateral properties of ht-29/b6 and ipec-j2 cell layers by impedance spectroscopy, mathematical modeling and machine learning. *PLOS ONE*, 8(7).

Schmid, T., Günzel, D., and Bogdan, M. (2013b). Efficient prediction of x-axis intercepts of discrete impedance spectra. In *Proceedings of the 21st European Symposium on Artificial Neural Networks, Computational Intelligence and Machine Learning (ESANN)*.

APPENDIX

A: Univariate Statistical Parameters

As described in the methods section, for each of the initial feature sets (S_ϕ, S_r, $S_\Re$, $S_\Im$) and therefrom derived feature sets ($S_{\Delta\phi}$, $S_{\Delta r}$, $S_{\Delta\Re}$, $S_{\Delta\Im}$, S_δ, S_δ) 16 univariate parameters were calculated:

1. minimum
2. first quartile
3. median
4. average
5. third quartile
6. maximum
7. standard deviation
8. variance
9. range
10. distance between median and average
11. interquartile distance
12. first percentile
13. ninth percentile
14. interpercentile
15. geometric mean
16. harmonic mean

B: Features of Subset C

In order to complete our report, we list the 23 features of subset C, which performed best among all subsets for the target range 1 to 10:

1. first quartile of $S_\Re$
2. maximum of $S_{\Delta\Re}$
3. maximum of $S_\Im$
4. range of S_ϕ
5. third quartile of $S_{\Delta\phi}$
6. maximum of $S_{\Delta\phi}$
7. variance of $S_{\Delta\phi}$
8. range of $S_{\Delta\phi}$
9. distance between mean and median of $S_{\Delta\phi}$
10. distance between first and ninth percentile of $S_{\Delta\phi}$
11. maximum of mean-normalized S_ϕ
12. ninth percentile of mean-normalized S_ϕ
13. maximum of mean-normalized $S_{\Delta\phi}$
14. interquartile range of mean-normalized $S_{\Delta\phi}$
15. range of median-normalized $S_{\Delta\phi}$
16. minimum of $S_{\overleftarrow{\delta}}$
17. first quartile of $S_{\overleftarrow{\delta}}$
18. third quartile of $S_{\overleftarrow{\delta}}$
19. maximum of $S_{\overleftarrow{\delta}}$
20. standard deviation of $S_{\overleftarrow{\delta}}$
21. range of $S_{\overleftarrow{\delta}}$
22. first percentile of $S_{\overleftarrow{\delta}}$
23. interquartile range of $S_{\overleftarrow{\delta}}$